ACS OMEGA

http://pubs.acs.org/journal/acsodf

Article

Forecast of Phase Diagram for the Synthesis of a Complex for the Detection of Cr^{6+} Ions

Sumit Chaudhary, Ramanand Rai,* Kedar Sahoo, and Manoj Kumar

Cite This: *ACS Omega* 2022, 7, 7460−7471

Read Online

ACCESS | Metrics & More | Article Recommendations | Supporting Information

ABSTRACT: A new organic complex (ANNBA) was synthesized using the solvent-free, solid-state reaction involving anthranilamide (AN)−*m*-nitrobenzoic acid (NBA). The established phase diagram specifies the formation of a complex in a 1:1 stoichiometric ratio which melts congruently at 142 °C. The diagram also infers the formation of two eutectics, E_1 and E_2, on either side of the complex with their respective melting at 118 and 106 °C. The stability and novelty of the synthesized complex was confirmed by differential scanning calorimetry, powder X-ray diffraction, and spectroscopic FTIR, ^{1}H, and ^{13}C NMR studies. The significant thermodynamic parameters such as the heat of mixing, the entropy of fusion, the roughness parameter, the interfacial energy, and excess thermodynamic functions have been studied. The novel complex (ANNBA) material displayed intense fluorescent emission as compared to the parent and the other well-known fluorescent organic material "pyrene." The influence of solvent's polarity on the absorption and emission of the complex has been studied in different solvents. Herein, we have displayed remarkable affinity of the complex toward hexavalent chromium ions in water, affecting its fluorescent property. We have deployed the synthesized complex as a turn-off fluorescent sensor to detect the most hazardous hexavalent chromium ions in water for the first time.

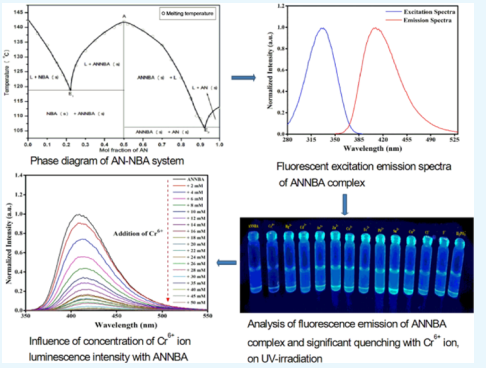

1. INTRODUCTION

The organic materials have been found to be promising and superior than inorganic materials for their various electronic and optoelectronic applications such as conductors, semiconductors, superconductors, light-emitting diodes, nonlinear optical materials, ferromagnetic materials, and optical sensors.[1−5] Over the last few decades, binary organic systems have shown importance in developing binary materials for thermal energy storage[6,7] and in designing pharmaceutical binary organic eutectic drugs, particularly by molecular association of different potential components of interest.[8−10] A promising application of binary organic materials has also been found for the multidrug therapy,[11−13] in which drugs are mixed together and the change in behavior of mixtures is studied. The materials' applications in binary organic systems, having electron donor and acceptor molecules, can be found in conductors, laser applications, and fluorescence probes.[1,14−16] The organic compounds containing the nitro group attached to the aromatic ring have been known for their versatile medical applications. The use of nitrofurazone ($C_6H_6N_4O_4$), chloramphenicol ($C_{11}H_{12}Cl_2N_2O_5$), nitrofurantoin ($C_8H_6N_4O_5$), and furazolidone ($C_8H_7N_3O_5$) are, respectively, known for the treatment of bacterial infections of the skin, cholera, urinary tract infections, and bacterial or protozoal diarrhea.[17−21] With a view of the usefulness of the binary organic complexes, we have chosen one parent component having a nitro group as *meta*-nitrobenzoic acid (NBA) which belongs to the monoclinic system with the centrosymmetric space group $P2_1/c$,[22] and another chosen parent component is anthranilamide (AN). The ANs containing the amide group have been used either as a starting compound or as an intermediate in the synthesis of significant biologically compounds such as quinazolone and benzoxazinones.[23,24] Moreover, the amides are good hydrogen-bond donors and hence capable of forming intermolecular hydrogen bonds with O-atoms or N-atoms of other hydrogen-bond acceptor compounds.[25] On the other hand, AN has already shown its application as a fluorescence label for the visualization of oligosaccharide materials.[26] The fluorescence materials for imaging are of immense importance, for the researchers, to be considered for investigations required for imaging in microbiology.

In view of the importance of binary materials for various applications and for fluorescence imaging in particular, the studies of compositional behavior of NBA and AN have been done in the entire range by the phase diagram investigation. The particular compositions of eutectics and the composition forming the intermediate compound, with novel behavior,

Received: August 10, 2021
Accepted: December 28, 2021
Published: February 21, 2022

have been identified. The materials' properties of significant compositions are being reported in detail. For establishing the phase diagram of the AN−NBA system as well as for the synthesis of the complex, the environment friendly solvent-free/solid-state synthesis route has been adopted. The structural changes of the complex have been studied using Fourier transform infrared (FTIR), Fourier transform nuclear magnetic resonance (FT-NMR), and powder X-ray diffraction (PXRD), and thermal behaviors of interesting compositions have been studied by differential scanning calorimetry (DSC) and differential thermal analysis (DTA) analysis. However, the studied optical property of the newly synthesized complex (ANNBA) shows a significantly enhanced fluorescence intensity than the well-known organic fluorescent pyrene as well as better than the parent compound. For plausible use of the complex as a fluorescent sensor, the studies were systematically extended to evaluate its applicability in the detection of environmental pollutants such as hexavalent chromium ions in water samples. It is one of the most harmful pollutants present in the groundwater and water bodies of Northern part of India (two districts, Unnao and Kanpur, in Uttar Pradesh which are in between Rishikesh and Varanasi). The major pollutants for Cr^{6+} are tanning industries, which discharge several tons of chromium (Cr^{6+}) over the permissible limits into the river water. An analysis of upstream and downstream water and sediments revealed a 10-fold increase in chromium levels in Ganga water, stretching right from Rishikesh to Varanasi. In this stretch, segments from Kannauj to Varanasi via Kanpur have been found to be the most polluted.[27] Some sensors have been developed for environmental pollutants, and advanced and smart materials that are environmental friendly have also been discovered.[28,29] However, such sensors are rare and mostly find application in gas sensing. In the present study, we report the synthesis of a novel organic complex in a single step using the "solid-state reaction method," with the 100% yield of the novel compound. The significant fluorescent property of the complex has been utilized to investigate for the environmental pollutant sensing purpose, and its efficiencies have been checked toward different metal ions (Cd^{2+}, Co^{2+}, Hg^{2+}, Mg^{2+}, F^{-}, Ca^{2+}, Cu^{2+}, Zn^{2+}, Cl^{-}, Sn^{2+}, and Fe^{2+}) in aqueous solution. Interestingly, the novel complex (ANNBA) displays selective behavior toward chromium (Cr^{6+}) ions present in the water samples and have been used as a turn-off fluorescent sensor. This significant finding of the complex in the present work is likely to open a new pathway to synthesize more novel complexes and to study other known organic biodegradable fluorescent materials[30,31] to be used as sensors.

2. RESULTS AND DISCUSSION

2.1. Phase Diagram. The phase diagram study is one of the significant techniques of materials science to study the properties and change in behavior of each and every composition. The diagram helps in identifying the composition forming the compound of novel behavior. Therefore, to study the phase diagram and compositional behavior, the binary mixtures of parent components (AN and NBA) were prepared in the entire range of composition, and the phase diagram was established. The melting temperature of all synthesized mixtures was determined, and the solid−liquid phase equilibrium curve was plotted in terms of melting temperature versus composition. The phase diagram of the AN−NBA system shows the formation of a complex (ANNBA) with a congruent melting temperature and two eutectics (E_1 & E_2) on either side of complex (Figure 1). The diagram clearly shows the compositional behavior reflecting in terms of change in their melting temperatures. On addition of AN to NBA, the melting temperature starts decreasing and acquires the minimum value of 119 °C called E_1 where the mole fraction of AN is 0.22. On further addition of AN, the melting temperature of the binary materials keeps on increasing and finally attains a maximum value of 142 °C for the complex (ANNBA), where the molar ratio of AN and NBA is 1:1, and this composition melts congruently. Beyond this composition, further addition of AN again causes the decrease in the melting temperature to its second minima, called E_2, at 106 °C where the mole fraction of AN is 0.92. Thereafter, on addition of AN, the melting temperature again increases and attains the melting temperature of AN. At the eutectic temperatures, the eutectic reaction occurs, which may be represented as

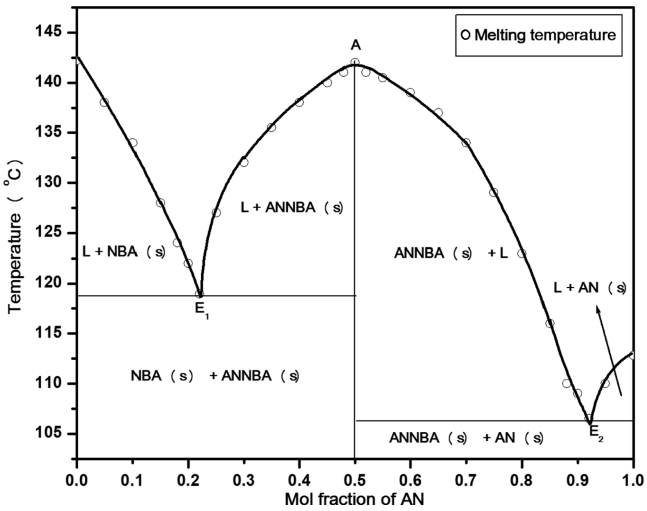

Figure 1. Phase diagram of the AN−NBA system.

$$L \rightleftharpoons +S_1 + S_2 \quad (1)$$

The above reaction shows that, at the eutectic temperature, the two solid phases are separated from its homogeneous liquid phase. The points E_1 and E_2 are invariant points and have zero degree of freedom.

2.2. Spectral Analysis. *2.2.1. IR Absorption. 2.2.1.1. FTIR Spectra of AN.* The band observed at 3412 cm^{-1} is primarily due to the NH_2 stretching of the aromatic primary amine. The two bands appearing at 3324 and 3198 cm^{-1} are asymmetric and symmetric stretchings of N−H in ($-CONH_2$). The peak at 1660 cm^{-1} is the characteristic (C═O) stretch. The C−N stretching and N−H bending vibrations are at 1258 and 1586 cm^{-1}, respectively. The peak assigned at 1629 cm^{-1} is due to NH_2 scissoring.

2.2.1.2. FTIR Spectra of NBA. The bands observed between 2552 and 3096 cm^{-1} are due to −OH stretching of the −COOH group. The sharp intense band at 1693 cm^{-1} is the characteristic of −C═O stretching. Asymmetric and symmetric stretchings of the ($-NO_2$) band are observed at 1531 and 1354 cm^{-1}, respectively. The bands observed at 1585 and 1417 cm^{-1} are indicative of the −C═C aromatic stretch. The C−N stretching and C−O stretching vibrations occur, respectively, at 1151 and 1294 cm^{-1}. The peaks at 926 and 723 cm^{-1} are attributed to OH and NO_2 bending vibrations.

2.2.1.3. FTIR Spectra of Complex (ANNBA). The recorded spectra for the synthesized novel organic complex show that some of the bands of parents remained as such, while there are

https://doi.org/10.1021/acsomega.1c04282
ACS Omega 2022, 7, 7460−7471

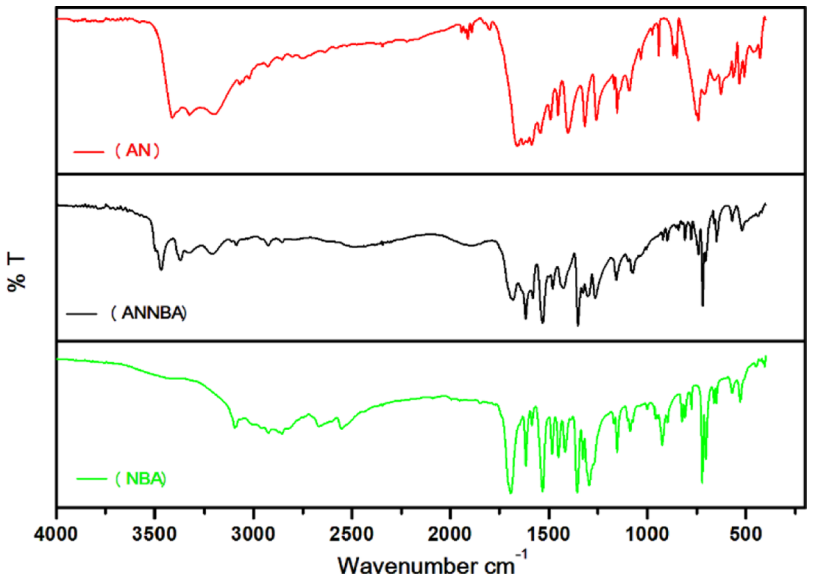

Figure 2. FTIR spectra of AN, NBA, and complex (ANNBA).

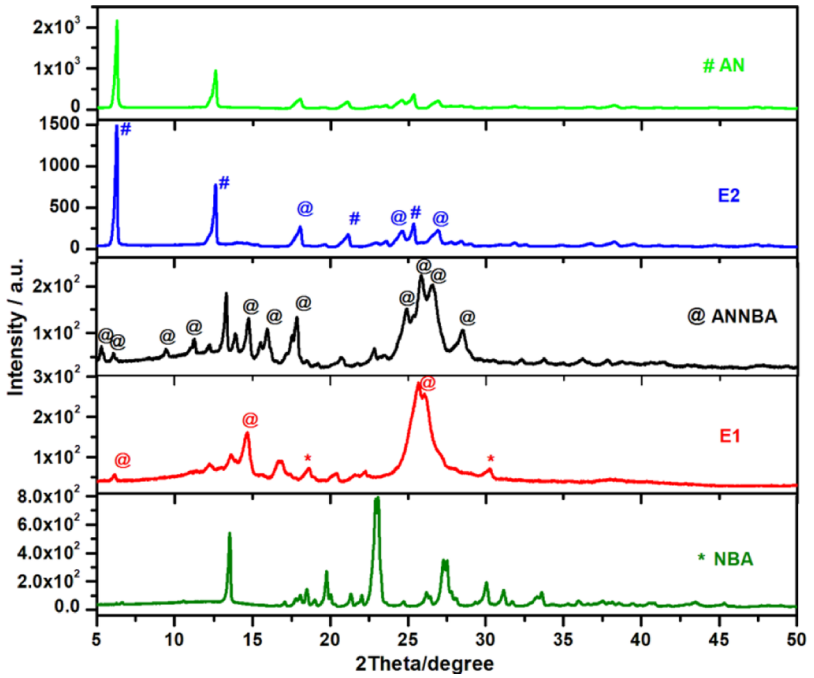

Figure 3. PXRD pattern of the AN−NBA system.

changes in their vibrational frequencies of some of the bands. The peak observed at 3412 cm^{-1} of the NH_2 group of AN is observed at 3469 cm^{-1} in the complex. The bands of AN observed at 3324 and 3198 cm^{-1} for the −NH stretch of $-CONH_2$ shifted to a higher wave number and appeared in the complex at 3370 and 3208 cm^{-1}, respectively. However, there is no significant change in the vibrational frequencies of $-NO_2$ asymmetric and symmetric stretchings (1530 and 1351 cm^{-1}). The strong peak at 1681 cm^{-1} corresponds to −C═O stretching and lies in between the −C═O stretching peaks of AN and NBA. Some bands appear in the region 2493 to 2950 cm^{-1}, and the shifts in the peaks of −NH and −C═O are indicative of the presence of intermolecular hydrogen bonding between AN and NBA in the complex. The FTIR spectra of AN, NBA, and complex (ANNBA) are depicted in Figure 2.

2.2.2. NMR Analysis. The FT-NMR spectra of AN, NBA, and complex were recorded in DMSO-d_6 and are discussed here.

2.2.2.1. AN. The ^{1}HNMR spectrum (Supporting Information S2a) shows seven peaks as δ 7.66 (br s, 1H), δ 7.46 (d, 1H), δ 7.08 (t, 1H), δ 7.00 (br s, 1H), δ 6.61 (d, 1H), δ 6.51 (br s, 2H), and δ 6.42 (t, 1H).[32] Its ^{13}C spectrum (Supporting Information S2b) also shows seven peaks for the respective skeletal as δ 171.81 for the carbonyl carbon, δ 150.71 for the carbon at which the NH_2 group is directly attached, δ 132.39 for C_5, δ 129.26 for C_7, δ 116.90 for C_6, δ 114.87 for C_2, and δ 114.19 for C_4.

The ^{1}HNMR spectrum (Supporting Information S3a) shows four signals for the corresponding protons as δ 8.57 (s, 1H), δ 8.42 (d, 1H), δ 8.29 (d, 1H), and δ 7.77 (t, 1H). The ^{13}C spectrum (Figure S3b) shows seven peaks as δ 166.05 for carbonyl carbon at C_1, δ 148.42 for C_3 carbon to which the

https://doi.org/10.1021/acsomega.1c04282
ACS Omega 2022, 7, 7460−7471

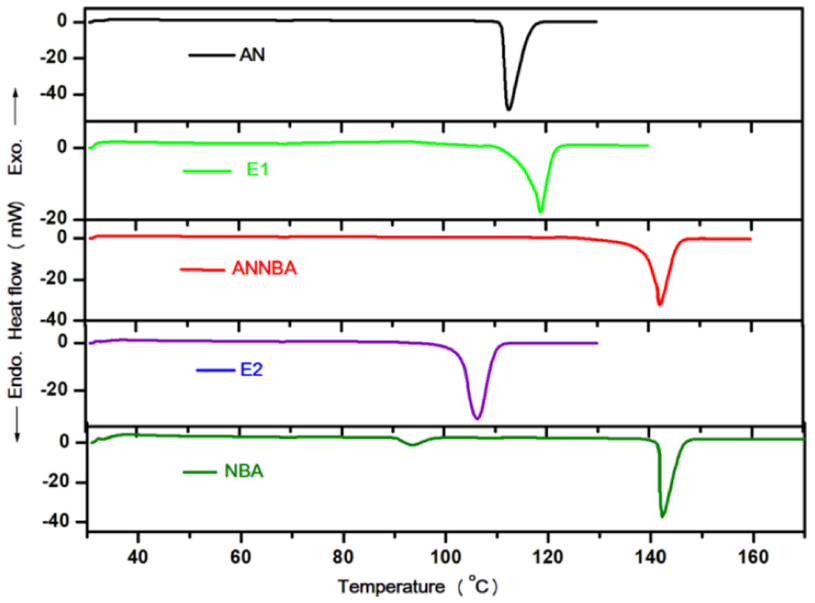

Figure 4. DSC plot of the AN−NBA system.

Table 1. Melting Temperature, Heat of Fusion, Heat of Mixing, and Entropy of Fusion of the AN−NBA System

component	melting temperature (K)	heat of fusion (kJ mol^{-1})	heat of mixing (kJ mol^{-1})	entropy of fusion (kJ mol^{-1} K^{-1})
AN	385.82 ± 0.5	21.54 ± 0.01		0.06 ± 0.001
NBA	415.19 ± 0.5	20.62 ± 0.01		0.04 ± 0.001
eutectic-1	391.96 ± 0.5			
(exp.)		19.54 ± 0.01	−11.04 ± 0.01	0.04 ± 0.001
(cal.)		30.58 ± 0.01		
eutectic-2	379.49 ± 0.5			
(exp.)		24.59 ± 0.01	−0.42 ± 0.01	0.06 ± 0.001
(cal.)		25.01 ± 0.01		
ANNBA (1:1)	415.14 ± 0.5	43.26 ± 0.01		0.14 ± 0.001

−NO_2 group is attached, δ 135.90 for C_6, δ 133.00 for C_7, δ 131.09 for C_5, δ 127.88 for C_4, and δ 124.21 for C_2.

2.2.2.3. Complex (ANNBA). In the ^{13}CNMR spectra, 14 peaks appear corresponding to different carbon atoms present in the complex, and their chemical shift values are δ 171.79, δ 166.09, δ 150.71, δ 148.41, δ 135.90, δ 133.36, δ 132.39, δ 131.03, δ 129.26, δ 127.75, δ 124.19, δ 116.90, δ 114.86, and δ 114.19. The ^{1}HNMR spectra shows 10 signals having chemical shift values as δ 8.62 (br s, 1H), δ 8.45 (d, 1H), δ 8.34 (d, 1H), δ 7.81 (t, 1H), δ 7.71 (s, 1H), δ 7.51 (d, 1H), δ 7.12 (t, 1H), δ 7.04 (br, s), δ 6.66 (d, 1H), and δ 6.47 (t, 1H). The proton and ^{13}C NMR spectra of the complex have been shown in Supporting Information S4a and b, respectively. The given NMR data in the manuscript do not reveal the nature of hydrogen bonding of the formed ANNBA complex.

2.2.3. PXRD Analysis. PXRD is one of the significant techniques to study the crystallinity of materials, identification of the crystalline phases, spacing between lattice planes, and novelty of the synthesized compound as well.[33] The recorded PXRD pattern with the newly synthesized complex, parent components (AN and NBA), and eutectics (E_1 and E_2) are depicted in Figure 3. It is evident from the figure that some new peaks, which could not be assigned for the PXRD pattern of parents AN and NBA, have appeared in the XRD pattern of the complex. The appearance of new peaks and the change in intensity of some of the peaks of the parents suggest the formation of a new entity.[34] While in the case of eutectics, the XRD pattern of E_1 shows either the peaks of NBA or the peaks of ANNBA, XRD of E_2 shows either the peaks of AN or the peaks of ANNBA. The existence of new peaks in the XRD pattern of the complex (ANNBA) suggests that the complex is entirely a new entity and is of crystalline nature; however, the existence of XRD peaks of either of the parent components or complex (ANNBA) in the XRD of eutectics (E_1 or E_2) confirm that the eutectics are of the same nature as the mechanical mixtures.

2.3. Thermal Analysis. *2.3.1. Enthalpy of Fusion and Thermochemistry.* In order to understand the thermal behavior, feasibility of the reaction, phase transitions, and other thermodynamic parameters, the DSC studies of the parent components, eutectics, and the novel complex have been done. The DSC curves of the pure components, the eutectics, and the complex are given in Figure 4. The experimental enthalpy of fusion values, which help in understanding the mechanism of solidification, the structure of the eutectic melt, and the nature of interaction between the components forming the eutectics and the complex, have been determined from DSC. The experimentally determined values of enthalpy of fusion and the theoretical values, calculated using the mixture law, are given in Table 1. The values of enthalpy of mixing for samples were obtained by subtracting the calculated values of enthalpy of fusion from the experimentally determined values. Based on the enthalpy of mixing values, three types of structures are suggested: quasi-eutectic for $\Delta H_{mix} > 0$, clustering of molecules for $\Delta H_{mix} < 0$, and molecular solution for $\Delta H_{mix} = 0$. The highly

https://doi.org/10.1021/acsomega.1c04282
ACS Omega 2022, 7, 7460−7471

negative values of enthalpy of mixing for both the eutectics suggest that there is associative interaction in the molecules forming the eutectic melt. The positive values for the entropy of fusion in all cases suggest that the process of melting favors.

Other thermodynamic information, such as the interfacial energy, the roughness parameter, and the grain boundary energy, which help in crystal growth and significantly influence the morphology of the crystal were also calculated using heat of fusion values. The interfacial energies were calculated by using the formula[35]

$$\sigma = \frac{C\Delta_{fus}H}{(N_A)^{1/3}(V_M)^{2/3}} \quad (2)$$

where N_A is the Avogadro number, V_M is the molar volume, and parameter C is a constant lying between 0.30 and 0.35. The value of C used for calculation was 0.35. The values of interfacial energies are given in Table 2. The Jackson's roughness parameter was studied using the following relation

$$\alpha = \frac{\xi\Delta_{fus}H}{RT} \quad (3)$$

where ξ is a crystallographic factor which is generally equal or less than1; for the present calculation, it is taken as 1, and the values are tabulated in Table 2.

Table 2. Roughness Parameter (α), Interfacial Energy (σ), and Grain Boundary Energy (γ) of AN, NBA, Eutectics, and AN−NBA (1:1)

component	α	σ (erg cm^{-2})	γ (erg cm^{-2})
AN	6.71	38.78	77.56
NBA	5.98	36.82	73.64
eutectic-1	5.98	37.25	74.51
eutectic-2	7.79	38.62	77.25
ANNBA (1:1)	17.16	37.80	75.61

2.3.2. Excess Thermodynamic Function. To understand the deviation from ideal behavior of eutectics and the nature of interactions existing between the components forming the eutectics, the excess thermodynamic functions in terms of excess free energy (g^E), excess enthalpy (h^E), and excess entropy (s^E) were studied by using the equations mentioned earlier.[31] The positive value of excess free energy suggests that there is a strong interaction between the like molecules forming the eutectic at E_1 and eutectic at E_2. The values of g^E, h^E, and s^E for both the eutectics are tabulated in Table 3.

Table 3. Excess Thermodynamic Functions for the Eutectics of the AN−NBA System

component	g^E (kJ mol^{-1})	h^E (kJ mol^{-1})	s^E (J mol^{-1} K^{-1})
eutectic-1	0.52	−6.76	−0.01
eutectic-2	0.50	19.31	0.04

2.4. Optical Studies. *2.4.1. UV−Visible Absorption Spectra.* To study the absorption spectra of the complex (ANNBA) and its parent components, AN and NBA were dissolved in ethanol to prepare 1 ppm solution at room temperature, and the spectra were recorded from 190 to 900 nm. In the UV−vis spectrum of *m*-NBA, two bands appear, first having a strong intensity at 215 nm due to n−σ* transition and the second having a weak intensity at 256 nm due to π−π* transition. For AN, three bands appear at 212, 248, and 331 nm which are, respectively, due to n−σ*, π−π* and n−π* transitions. In the case of the synthesized complex, three bands appear similar to that of AN, but the absorption intensity increases which infers the hyperchromicity and sensitivity to hydrogen bonding.[36] The recorded absorption spectra of the complex along with parent components are shown in Figure 5a.

2.4.2. Emission Spectra. The emission spectra of the ANNBA complex along with its parent components are depicted in Figure 5b. The emission spectra were recorded by exciting with their respective λ_{max}. NBA did not show any noticeable fluorescence emission upon excitation, while AN shows a remarkable fluorescence intensity at 410 nm, that is, in the blue region. However, the complex shows significant intense fluorescence as compared to AN in the same region.

In order to study the importance of the newly synthesized complex (ANNBA) for its fluorescence emission, comparative fluorescence studies of ANNBA to that of well-known standard organic fluorescence material, pyrene, have been done with the identical concentration solutions of ANNBA and pyrene. The synthesized novel ANNBA on excitation with 250 nm shows significant intense and promising fluorescence emission, and its intensity was found to be greater than thrice that of pyrene (Figure 6a). When the synthesized novel ANNBA was excited with 330 nm, the observed emission intensity was also found promising and comparable to the fluorescence observed on excitation with 250 λ_{max}, and its intensity is still 2.5 times greater than that of pyrene. Two particular observations of ANNBA emission have been noted with 330 λ_{max}: first, the wavelength of maximum emission red-shifted with broadening, and second, the emission intensity slightly decreased as compared to excitation at 250 nm (Figure 6b).

To study the influence of polarities of solvents on the emission of the complex, the absorption and emission spectra of the complex (ANNBA) with its λ_{max} excitation in different solvents of different polarities were also studied in selected solvents [methanol, ethanol, acetonitrile, ethyl acetate, and tetrahydrofuran (THF)] and are depicted in Figure 7a,b, respectively. The observation of promising fluorescence emission with the newly synthesized complex opens the road map for the study of its possible application to be used for sensing the environmental pollutants.

2.4.3. Solvatochromism. The influences of polarities of solvents on the fluorescence emission of the complex (ANNBA) have found to be red-shifted from the nonpolar solvent to the highly polar solvent, whereas in the case of absorptions, the polarity effect does not follow the order of sequence. This indicates that the fluorescence transitions are much more sensitive toward the polarity of the solvent than the absorption. The observed Stoke's shift value for the complex in different solvents shows an ordered pattern and increases from polar (ethanol) to moderately polar THF which exhibits its sensitive behavior toward different solvents. The finding is clearly apparent from Table 4. The observed large shifting explains that when an electron-donating group (amino group) and an electron accepting group (carbonyl group) combines either directly or through a bridge of conjugated double bonds, the migration of electrons is possible from the former to the latter, and subsequently, the complex gives rise to a special absorption band totally different from the parent components.[37−39] The variation in the absorption maxima and the fluorescence have been plotted in terms of Lippert−Mataga solvent polarity

https://doi.org/10.1021/acsomega.1c04282
ACS Omega 2022, 7, 7460−7471

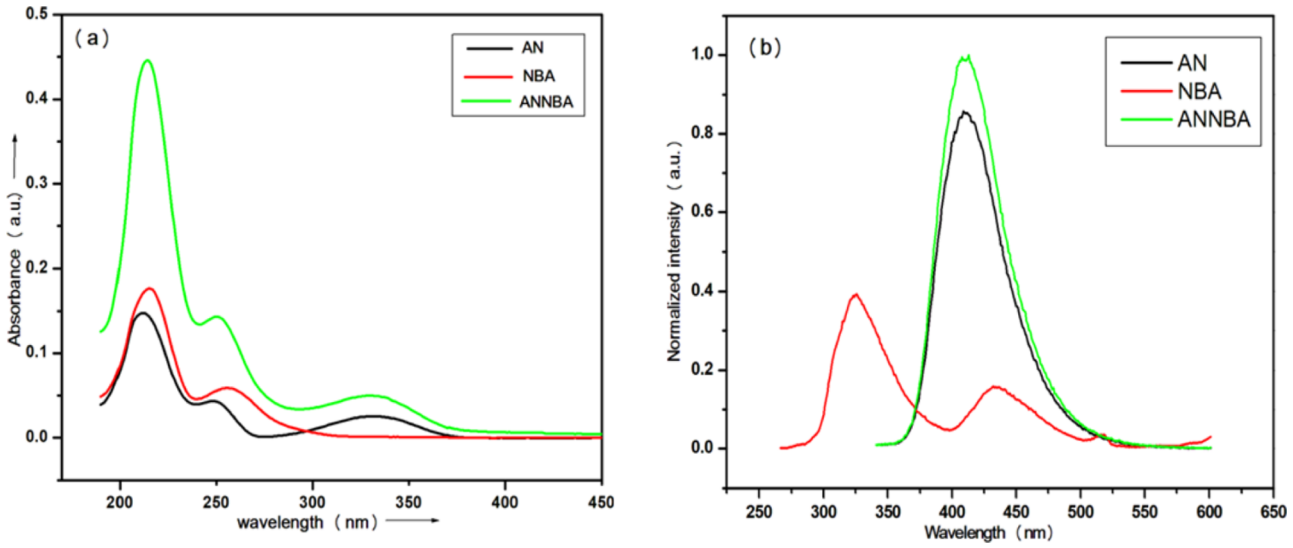

Figure 5. (a) UV−vis and (b) emission spectra of ANNBA, AN, and NBA in ethanol.

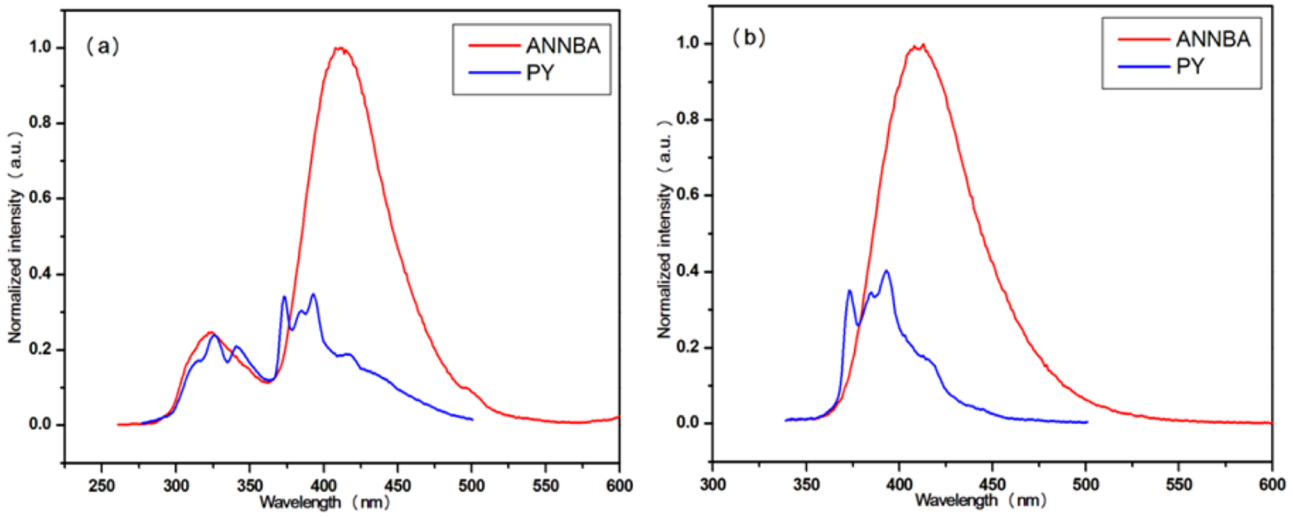

Figure 6. (a) Emission spectra of ANNBA vs pyrene at 250 nm. (b) Emission spectra of ANNBA vs pyrene at 330 nm.

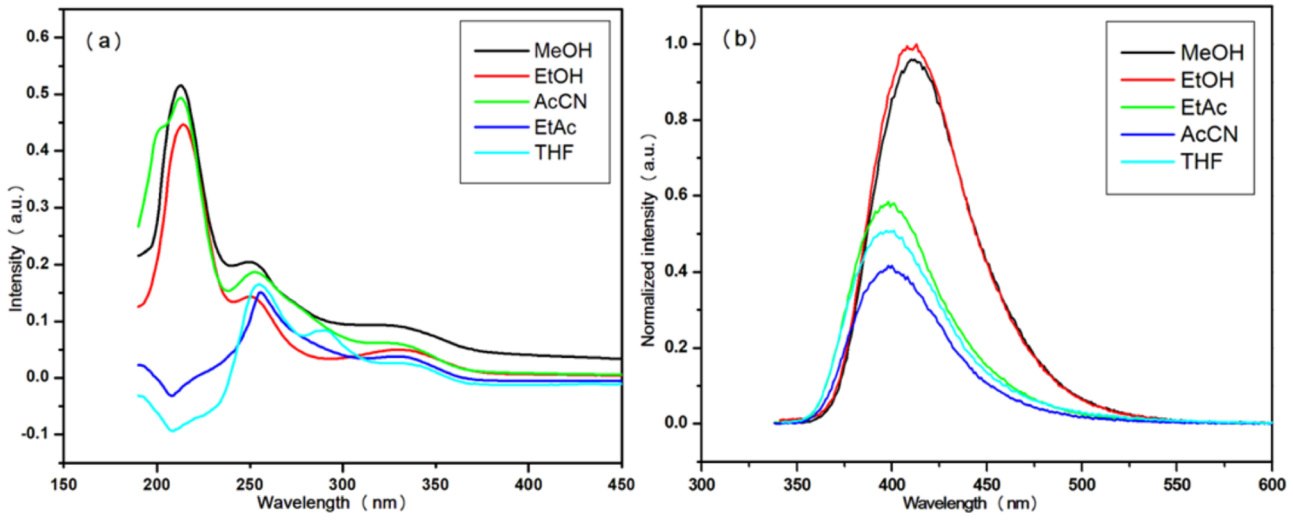

Figure 7. (a) UV−vis spectra of ANNBA in different solvents. (b) Emission spectra of ANNBA in different solvents.

https://doi.org/10.1021/acsomega.1c04282
ACS Omega 2022, 7, 7460−7471

Table 4. Wavelength of Maximum UV−Vis Absorption and Fluorescence, Stoke's Shift of Complex in Different Polar Solvents, and Solvent Polarity Function

S no.	solvent	absorption λ_{max} (nm)	fluorescence λ_{max} (nm)	Stoke shift (nm)	solvent polarity function (Δf)
1	methanol	328	411	83	0.3927
2	ethanol	331	412	81	0.3796
3	ethyl acetate	328	397	69	0.2924
4	acetonitrile	328	400	72	0.3937
5	tetrahydrofuran	332	396	64	0.3090

parameter (Δf) which is a function of the dielectric constant (ε) and refractive index (η) of the solvents.[40,41]

$$\Delta f = f(\eta) - \frac{1}{2} f(\eta)^2 \tag{4}$$

where

$$f(\varepsilon) = \left[\frac{(\varepsilon - 1)}{(2\varepsilon + 1)}\right] \text{and} f(\eta)^2 = \left[\frac{(\eta^2 - 1)}{(2\eta^2 - 1)}\right] \tag{5}$$

The linear variation of absorption and emission maxima with the solvent polarity function (Δf) shown in Lippert−Mataga plot (Figure 8) is indicative that the hydrogen-bonded complexes are sensitive toward the polarity of the solvents.[42]

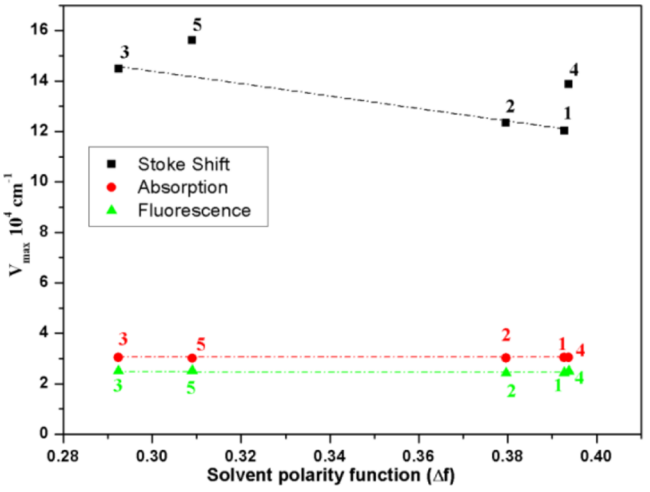

Figure 8. Lippert−Mataga plots of absorption; fluorescence and Stoke's shift against the solvent polarity function (Δf) of the complex in (1) methanol, (2) ethanol, (3) acetonitrile, (4) ethyl acetate, and (5) THF.

2.5. ANNBA as a Turn-Off Fluorescent Sensor for Cr^{6+} Detection. The synthesized complex (ANNBA), when excited at 330 nm, displayed a Stoke's shift of ~82 nm, with an emission maximum of 412 nm (Figure 9). For the estimation of hexavalent chromium in ground water through development of a fluorescent sensor, the emission intensity at 412 nm (maxima) was used. Upon addition of [Cr^{6+}] to the solution containing the complex, the emission was quenched, which is explicitly visible by naked eyes under UV irradiation (Figure 10).

Notably, with the decrease in ANNBA emission, I_{signal} corresponding to the concentration of chromium in aqueous solution increases. This increase in I_{signal} occurs due to the signal processing (ref to eq 6). Furthermore, on addition of Cr^{6+} ions

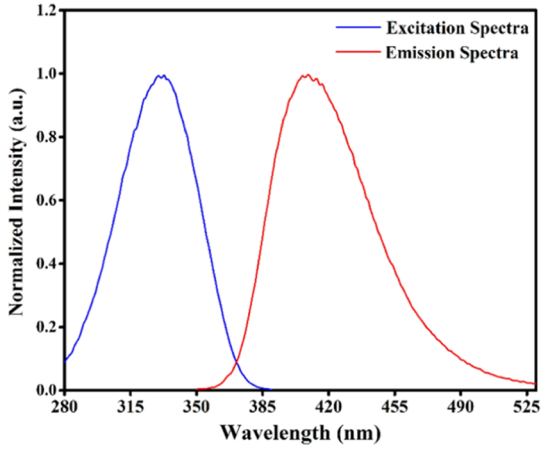

Figure 9. Excitation and fluorescent emission spectra of the ANNBA complex.

to the solution containing ANNBA, it was allowed to equilibrate for 10−15 min. For the quantitative estimation of hexavalent ions in the ground water, the linear increase in I_{signal} as a function of the chromium concentration was evaluated.

$$I_{signal} = 1 - (I_i/I_{blank}) \tag{6}$$

I_i = intensity of ANNBA after addition of the metal analyte; I_{blank} = raw emission intensity of ANNBA; I_{signal} (eq 6) is plotted against the Cr^{6+} concentration.

It was observed that for serially diluted (2−50 mM) hexavalent chromium solutions, the fluorescent emission of ANNBA gradually decreased (Figure 11a), whereas the I_{signal} increased gradually when the concentration of the Cr^{6+} ions varied from 2 to 50 mM as shown in Figure 11b. Figure 11a displays a gradual decrease in fluorescence emission and a subsequent rise in the I_{signal} (Figure 11b) with an increase in the hexavalent chromium concentration (2 to 50 mM). Note, that the linear region of the calibration curve (Figure 11b inset) is used to estimate the unknown concentration of chromium in the synthetic ground water sample, in this study.

Furthermore, the sensor selectivity toward hexavalent chromium ions in the solution was evaluated (Figure 12a) by screening Cd^{2+}, Co^{2+}, Hg^{2+}, Mg^{2+}, F^-, Ca^{2+}, Cu^{2+}, Zn^{2+}, Cl^-, Sn^{2+}, and Fe^{2+} against the fixed concentration of ANNBA using the outlined protocol provided in the Experimental Section. It was observed that fluorescence emission of the complex (ANNBA) is significantly quenched (I_{signal} increased) in the case of Cr^{6+} and to some extent in the case of Sn^{2+} and Cu^{2+}. However, this quenching is significantly small as compared to Cr^{6+}, which is also visible via naked eyes (Figure 10), while for other ions (Cd^{2+}, Co^{2+}, Hg^{2+}, Mg^{2+}, F^-, Ca^{2+}, Cu^{2+}, Zn^{2+}, Cl^-, Sn^{2+}, and Fe^{2+}), I_{signal} is found to decrease. It is important to mention here that with the addition of the interfering ions (Cd^{2+}, Co^{2+}, Hg^{2+}, Mg^{2+}, F^-, Ca^{2+}, Cu^{2+}, Zn^{2+}, Cl^-, Sn^{2+}, and Fe^{2+}), ANNBA emission increased (Supporting Information S6) leading to a decrease in I_{signal} (Figure 12a).

To keep the presentation of the data simple, the I_{signal} change for interfering ions is presented at a single concentration, and an interesting observation with Cr^{6+} has been exploited for its further study in detail. It is worth noticing that ANNBA behaves very different when treated with interfering ions as compared to Cr^{6+} ions. Two mechanisms, viz, (i) electron transfer and (ii) fluorescence resonance energy transfer (FRET), can be responsible for such behavior of the sensor. To delineate the

https://doi.org/10.1021/acsomega.1c04282
ACS Omega 2022, 7, 7460−7471

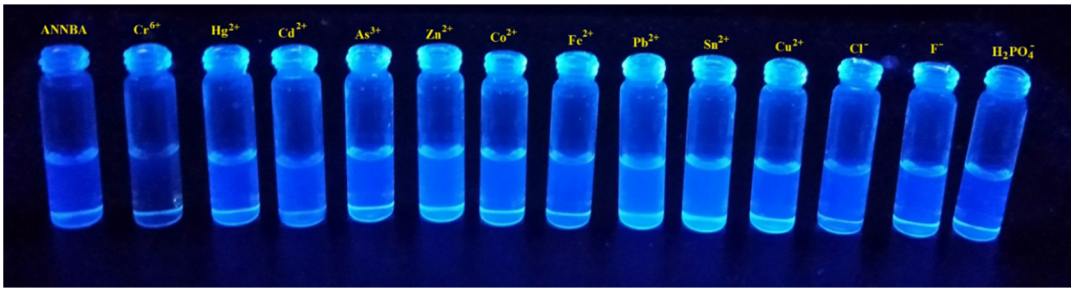

Figure 10. Analysis of fluorescence emission of the ANNBA complex and significant quenching with Cr^{6+} ion, on UV-irradiation, which is not reflected with other analytes.

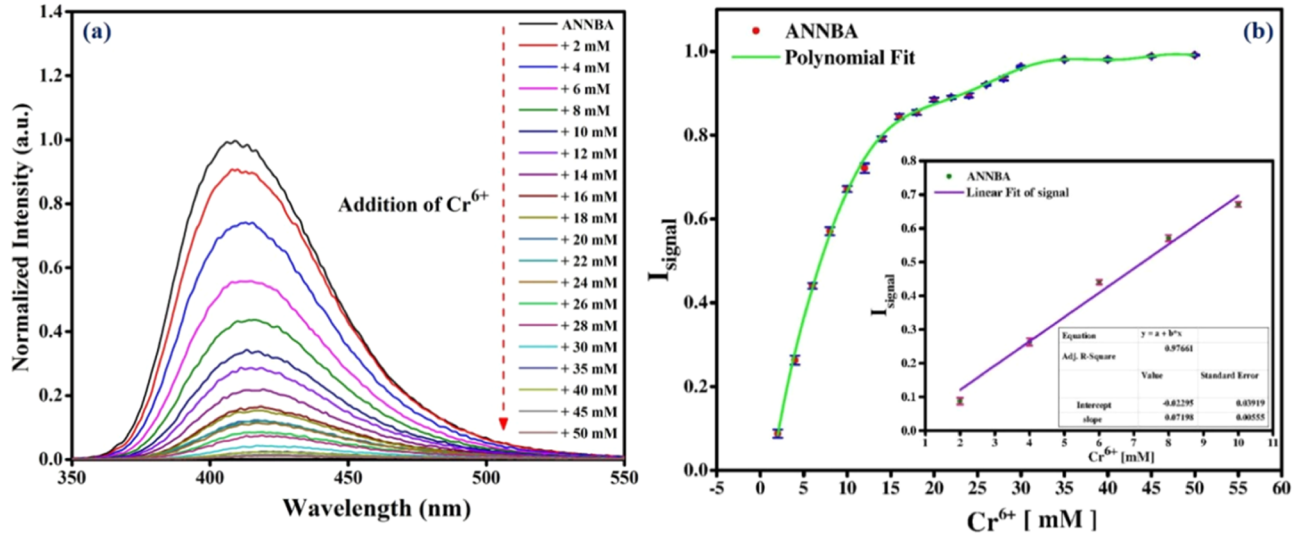

Figure 11. (a) Influence of concentration of Cr^{6+} ion on the luminescence emission intensity with ANNBA. (b) Fluorescent signal calculation in the Cr^{6+} concentration range of 2−50 mM. Polynomial curve elucidating the linear calibration curve within the range 2−10 mM (inset).

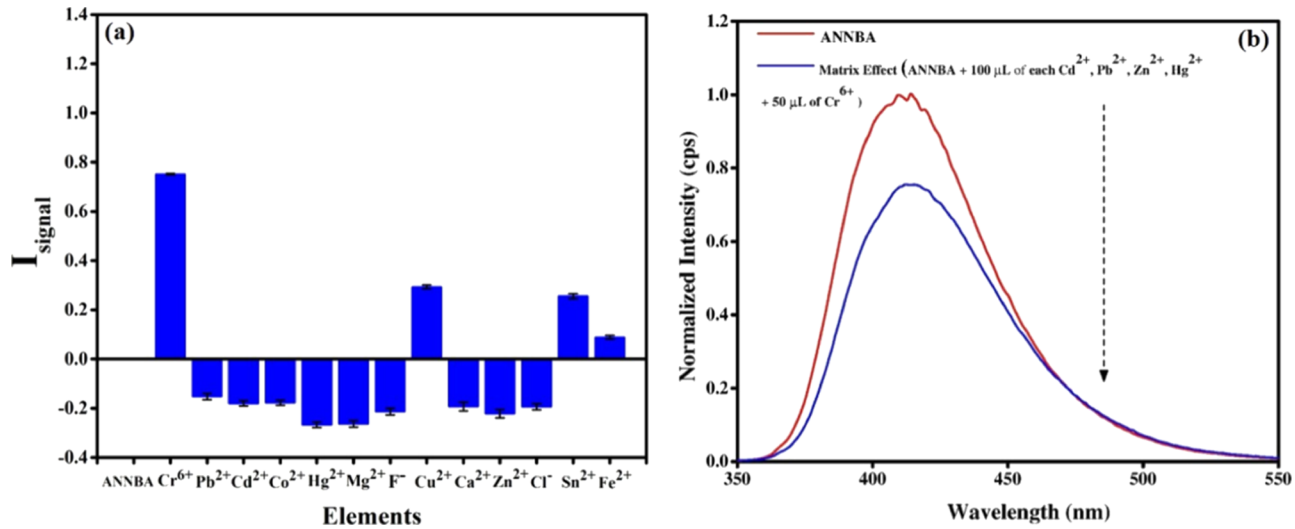

Figure 12. (a) Selectivity of the developed ANNBA sensor toward the Cr^{6+} ion. (b) Matrix effect representing ultrasensitivity of ANNBA toward Cr^{6+} ion even in the presence of 100 μL each of Cu^{2+}, Pb^{2+}, Zn^{2+}, and Hg^{2+}.

sensing mechanism, change in absorption spectra of ANNBA as a function of ion concentration (Cr^{6+}/interfering ions) was recorded.

On close observation of Figure 13a, it is observed that no significant shift in absorption spectra occurred, ruling out the role of electron transfer in the detection mechanism. This indicates that fluorescence quenching is possibly due to FRET. Occurrence of this phenomenon can be evaluated by verifying the overlap between the absorption spectra of the acceptor (in the ground state) and the emission spectra of the donor (in the excited state). The occurrence of FRET at a very short donor and acceptor separation distance (10 nm) makes this method

https://doi.org/10.1021/acsomega.1c04282
ACS Omega 2022, 7, 7460−7471

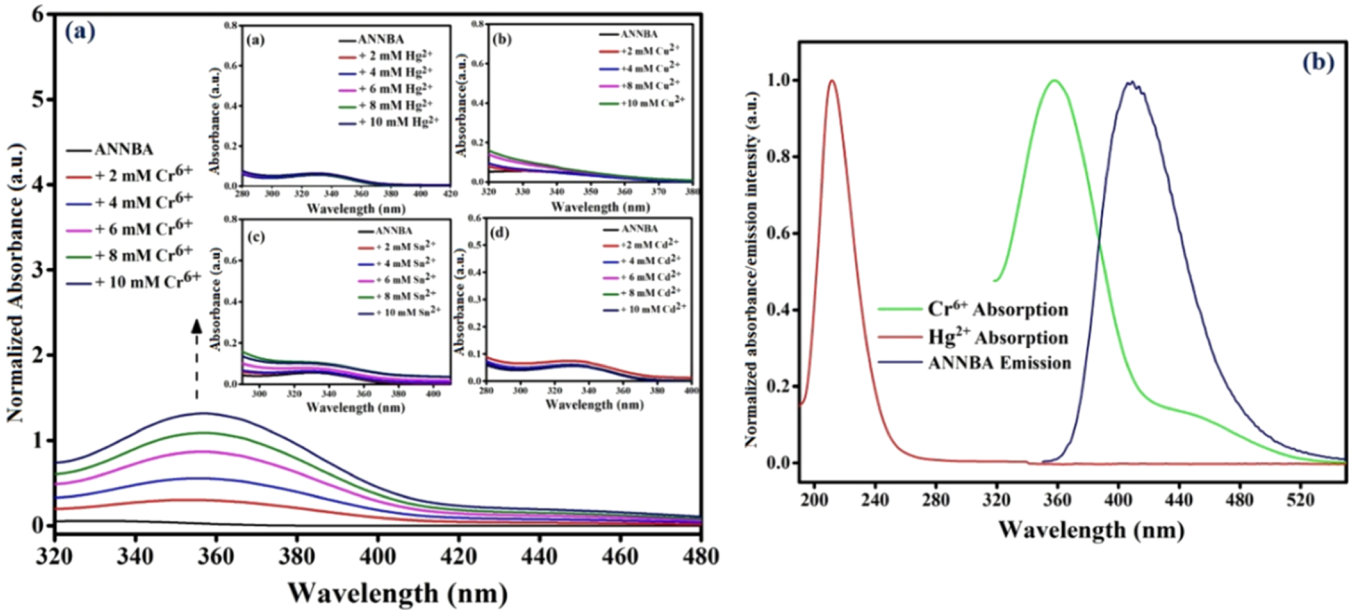

Figure 13. (a) Regular increase in the optical absorption spectra of ANNBA at different mM Cr^{6+} ions. Inset showing nearly unchanged or random variation of absorption band in the presence of Hg^{2+}, Cu^{2+}, Sn^{2+}, and Cd^{2+}ions. (b) Spectral overlapping of the absorption intensity of Cr^{6+} ions with the emission intensity of ANNBA, indicating the plausible energy transfer process. Same is not visible in the case of Hg^{2+} ion.

very selective and sensitive. It is well known that FRET does not require an acceptor to be fluorescent.[43] Besides, emission and reabsorption of photons do not take place during this process. However, similar to FRET, another competing mechanism such as radiative energy transfer is known to exhibit a similar effect. However, this can be easily excluded by performing the experiments at lower absorbance values (less than 0.1). As the FRET occurs, a subsequent decrease in donor emission and an increase in acceptor emission (only when acceptor is fluorescent) becomes evident. This phenomenon occurs due to exchange of energy from the oscillating dipole of the donor to the acceptor.[44]

Interestingly, Figure 13b shows a significant overlap (overlapping area: ~42) between the absorption spectra of Cr^{6+} and the emission spectra of the complex (ANNBA), indicating the probability of FRET. The absorption spectra of Cr^{6+} overlap with the emission spectra of ANNBA, designated as an acceptor and donor, respectively. Hence, upon addition of Cr^{6+} ions to the solution, a concomitant decrease in the emission spectra of ANNBA is observed due to the FRET mechanism (Figure 11a). The occurrence of FRET between the designated donor and acceptor again is supported by the fact that there is an effective interaction between ANNBA and Cr^{6+} ion as indicated in (Figure 13a). This effective interaction between ANNBA and Cr^{6+} ions can be visible from the increased ANNBA absorption spectra (Figure 13a) with a rise in the added Cr^{6+} concentration. It is important to mention here that Cr^{6+} acts like an acceptor, which is not intrinsically fluorescent. The increase in the optical absorption of ANNBA with the concentrated sample of Cr^{6+} ion as a result of effective interaction led to enhanced spectral overlapping between the acceptor and the donor. Thus, there are stronger chances of FRET to occur, which consequently decreases the emission of ANNBA (donor) and thus increases the I_{signal} value.

On the contrary, addition of some interfering ions (Cd^{2+}, Hg^{2+}, Cu^{2+}, and Sn^{2+}) to the solution (Figure 13a inset) leads to no noticeable change in the absorption spectra of ANNBA (in fact a slight decrease in absorption is noticed) coupled with the increase in the emission from the ANNBA. As the absorption decreases slightly, there is no significant change in the overall spectral overlap due to which FRET between the donor and acceptor becomes weak, and hence a slight increase in ANNBA emission (decrease in I_{signal}) is noticed (Figure 12a). This distinct and significant behavior of ANNBA is employed to distinguish the analyte from interfering ions (Figure 12a) which is certainly impressive. This capability can be further examined to check the sensor ability to detect the analyte even in the mixture of interfering ions.

Briefly, to the water sample consisting of Cd^{2+}, Pb^{2+}, Zn^{2+}, and Hg^{2+} ion mixture (each of 10 mM concentration and 100 μL), a predetermined concentration of Cr^{6+} (2 mM and 50 μL) was added, and a change in the ANNBA emission was noted. Interestingly, the ANNBA based sensor displayed quenched fluorescent emission (Figure 12b) (I_{signal} increased), indicating the sensor's ability to detect hexavalent chromium ions in the heavy metal mixed complex water samples.

The analytical parameters, viz., the theoretical limit of detection (LOD) and the limit of quantitation (LOQ = 10 × LOD), for the sensor to detect hexavalent chromium in the water samples are calculated in the dynamic range. It is found that the developed sensor is capable of detecting hexavalent chromium as low as (3σ value) 0.4 mM, whereas the LOQ for the developed sensor is found to be 4 mM. The performance of the newly developed ANNBA sensor toward hexavalent chromium is encouraging to explore other such biodegradable novel organic materials; nevertheless, there are several fluorescent sensors that have better performance toward hexavalent chromium.[45−47] However, current research certainly demonstrates the ability of ANNBA to detect hexavalent chromium in water samples for the first time.

3. CONCLUSIONS

A novel complex (ANNBA) of AN and NBA has been synthesized by adopting a green synthetic route of solvent-free

https://doi.org/10.1021/acsomega.1c04282
ACS Omega 2022, 7, 7460−7471

synthesis. The phase diagram study, which is a significant tool to study the compositional behavior of AN−NBA, infers that in the entire range of compositions, there are formations of two eutectics and a novel organic complex. The novelty and structural changes of the newly synthesized complex have been confirmed by the FTIR, NMR, PXRD, and DSC techniques. The optical properties of the novel complex and parent components were studied using UV−vis absorption and fluorescence emission. Significant intense fluorescence emission was recorded with newly synthesized complex. The intensity of fluorescence emission recorded with the newly synthesized complex was found to be greater than its parent compounds as well as 3 times greater than that of pyrene, which is a well-known organic fluorescent compound. The Lippert−Mataga study has suggested that the charge transfer is higher in the excited state than in the ground state. The remarkable fluorescence property of the newly synthesized complex has been exploited in detail. The fluorescence emissions of the complex in the presence of interfering ions (Cd^{2+}, Co^{2+}, Hg^{2+}, Mg^{2+}, F^{-}, Ca^{2+}, Cu^{2+}, Zn^{2+}, Cl^{-}, Sn^{2+}, and Fe^{2+}) were studied. The complex (ANNBA) shows marvelous affinity toward Cr^{6+} ions in water samples, and the observation indicated that it can be used as a (turn-off) fluorescent sensor. The developed ANNBA luminescent probe has a wide dynamic range (2−50 mM) concentration with the limit of linearity within 2−10 mM of Cr^{6+}. Our approach for synthesizing the novel biodegradable organic sensor materials using solvent-free solid-state reaction would be the novel opening for the designing of novel fluorescent organic sensors with better lower detection limit on applying some modification in the structure. Besides the synthesis of novel materials with 100% yield, the report will also be insisting to explore the fluorescent properties of known organic materials as well as to synthesize new promising materials in the future.

4. EXPERIMENTAL SECTION

4.1. Chemicals and Purification for Synthesis. The parent compounds NBA and AN were obtained from Sigma-Aldrich, Germany, having purity of 99 and 98%, respectively. The purity of both NBA and AN were checked by their melting points and NMR studies, and these were found in agreement with the values reported in the literature.[48]

4.1.1. Chemicals for Fluorescence Sensing. Chemicals procured from SRL Chemicals (sodium fluoride, tin chloride, cobalt sulphate, and ferrous sulphate), SDF Chemicals (sodium arsenite and nitric acid), Alfa Aesar (hydrofluoric acid, sodium fluoride, sodium chloride, and zinc chloride), Merck India Pvt. Ltd. (mercury chloride and lead chloride), Fisher Scientific (cadmium chloride and phosphoric acid), and Rankem (calcium chloride, magnesium chloride, potassium dichromate, and ferrous sulfate) were used as such without any further purification. Importantly, for the preparation of hexavalent chromium solution, protocols outlined in the American Public Health Association, the American Water Works Association, and the Water Pollution Control Federation have been employed.[49]

4.2. Phase Diagram Study. The phase diagram of the AN−NBA system was established in the form of the melting temperature-composition curve.[50] The mixtures of the parent component were prepared for the entire range of composition by weighing their appropriate amount using the balance of accuracy ±0.0001 g. The mixtures were taken in different test tubes, and the mouth of the test tubes was sealed to avoid contamination. The mixtures in test tubes were homogenized in silicon oil bath by repeating the process of melting and mixing followed by chilling in ice−cold water for four times. The melting points of these homogenized compositions were determined using a Toshniwal melting point apparatus attached with a thermometer which can read up to ±0.5 °C. The graph was plotted between the compositions and their corresponding melting temperatures along *X* and *Y* axes, respectively.

4.3. Thermal Study. The enthalpy of fusion values of parent components, their eutectics, and complex (ANNBA) were determined with the help of DSC (Mettler DSC-4000 system), which was calibrated using indium and zinc samples by taking the samples about 4−7 mg in a sealed aluminum pan. DTA and thermogravimetric analysis (TGA) were also performed for parents and complex using a PerkinElmer, STA 6000 system. For the thermal studies, DSC, DTA, and TGA, the samples were heated with a heating rate of 10 °C/min under a constant flow (20 mL/min) of nitrogen gas. The values of enthalpy of fusion were found to be reproducible within ±0.01 kJ/mol.

4.4. Spectral Study. The FTIR spectra of the parent components and the synthesized complex (ANNBA) were recorded by dispersing powder samples in KBr and pelletizing them. The spectrum of pellets was studied using a PerkinElmer FTIR spectrophotometer in the region of 4000−400 cm^{-1}. The ^{1}H and ^{13}C FT-NMR spectra of the samples were recorded using a JNM-ECZ500R/S1 500 MHz spectrometer in DMSO-d_6 solvent.

4.5. PXRD Study. The XRD pattern of the parent components, their eutectics, and complex were recorded using an 18 kW rotating (Cu) anode-based Rigaku powder diffractometer. The graphite was used as a monochromator. Each sample was recorded at a scanning rate of 4°/min.

4.6. Optical Study. The UV absorption spectra of the parent components and the complex (ANNBA) were recorded at 300 K with an identical concentration solution (1 ppm) in ethanol by employing a UV/Vis/NIR (JASCO model V-670) spectrometer from 190 to 1200 nm. However, the fluorescence emission spectra were recorded for the respective samples at the same temperature using a QM-400, Horiba Canada Fluorescence spectrometer, a step size of 0.5 nm, and an integration time of 0.1 s. The well-known standard organic fluorescence compound, pyrene, was used for the comparative studies of ANNBA fluorescence. The influences of polarity of solvents were also studied using the same spectrofluorometer.

4.7. Analyte Sensing Methodology. All chemicals (analytes) were prepared using the serial dilution method from 100 mM stock solution. The fluorescence spectra of ANNBA solution (10^{-5} M) in the ethanol solvent was recorded in the above-mentioned spectrofluorometer. Hexavalent chromium [Cr^{6+}] was added to the ANNBA solution sequentially ranging from 2 to 100 mM, and the resulting spectra were recorded. Further, an absorbance spectrum (250−500 nm) of ANNBA was also obtained using the same UV−vis spectrometer. The same procedure was adopted for other analytes as well.

■ ASSOCIATED CONTENT

Supporting Information

The Supporting Information is available free of charge at https://pubs.acs.org/doi/10.1021/acsomega.1c04282.

Reaction scheme and proposed structure of the solid-state synthesized compound; ^{1}HNMR and ^{13}C NMR of AN, NBA, and ANNBA in DMSO-d_6; TGA DTA curve of the novel complex (ANNBA); and emission comparison of

https://doi.org/10.1021/acsomega.1c04282
ACS Omega 2022, 7, 7460−7471

different analytes upon addition against the raw emission of ANNBA (PDF)

AUTHOR INFORMATION

Corresponding Author

Ramanand Rai − *Department of Chemistry, Institute of Science, Banaras Hindu University, Varanasi 221005, India;* orcid.org/0000-0003-1681-5098; Email: rn_rai@yahoo.co.in

Authors

Sumit Chaudhary − *Department of Chemistry, Institute of Science, Banaras Hindu University, Varanasi 221005, India*

Kedar Sahoo − *Department of Chemical Engineering, IIT BHU, Varanasi 221005, India*

Manoj Kumar − *Department of Chemical Engineering, IIT BHU, Varanasi 221005, India;* orcid.org/0000-0002-6278-781X

Complete contact information is available at: https://pubs.acs.org/10.1021/acsomega.1c04282

Notes

The authors declare no competing financial interest.

ACKNOWLEDGMENTS

The authors would like to thank the Head, Department of Chemistry, Banaras Hindu University for providing infrastructural facility, and one of the authors, S.C., would also like to thank CSIR, New Delhi for the research fellowship.

REFERENCES

(1) Inokuchi, H. Organic semiconductors, conductors and superconductors. *Int. Rev. Phys. Chem.* **1989**, *8*, 95−124.

(2) Rai, R. N.; Ramasamy, P.; Lan, C. W. Synthesis and crystal growth of binary organic NLO material UNBA. *J. Cryst. Growth* **2002**, *235*, 499−504.

(3) Thompson, J.; Blyth, R. I. R.; Mazzeo, M.; Anni, M.; Gigli, G.; Cingolani, R. White light emission from blends of blue-emitting organic molecules: a general route to the white organic light emitting diode. *Appl. Phys. Lett.* **2001**, *79*, 560−562.

(4) Escher, C.; Wingen, R. Ferroelectric Liquid Crystals in High Information Content Displays. *Adv. Mater.* **1992**, *4*, 189−197.

(5) Spangler, C. W. Recent development in the design of organic materials for optical power limiting. *J. Mater. Chem.* **1999**, *9*, 2013−2020.

(6) Pereira da Cunha, J.; Eames, P. Thermal energy storage for low and medium temperature applications using phase change materials − A review. *Appl. Energy* **2016**, *177*, 227−238.

(7) Atinafu, D. G.; Dong, W.; Huang, X.; Gao, H.; Wang, G. Introduction of organic-organic eutectic PCM in mesoporous N-doped carbons for enhanced thermal conductivity and energy storage capacity. *Appl. Energy* **2018**, *211*, 1203−1215.

(8) Klímová, K.; Leitner, J. DSC study and phase diagrams calculation of binary systems of paracetamol. *Thermochim. Acta* **2012**, *550*, 59−64.

(9) Cherukuvada, S.; Nangia, A. Fast dissolving eutectic compositions of two anti-tubercular drugs. *CrystEngComm* **2012**, *14*, 2579−2588.

(10) Shekhar, H.; Kumar, M. Phase Diagram, Thermodynamic Stability and Interfacial Studies on Solid Dispersions of Phenothiazine-Acetanilide Drug System. *Asian J. Org. Med. Chem.* **2016**, *1*, 26−32.

(11) Smith, C. S.; Aerts, A.; Saunderson, P.; Kawuma, J.; Kita, E.; Virmond, M. Multidrug therapy for lepsrosy: a game changer on the path to elimination. *Lancet Infect. Dis.* **2017**, *17*, e293−e297.

(12) Aguiari, G.; Catizone, L.; del Senno, L. Multidrug Therapy for Polycystic Kidney Disease: A Review and Perspective. *Am. J. Nephrol.* **2013**, *37*, 175−182.

(13) Backonja, M.-M.; Irving, G.; Argoff, C. Rational Multidrug Therapy in the Treatment of Neuropathic Pain. *Curr. Pain Headache Rep.* **2006**, *10*, 34−38.

(14) Wasielewski, M. R. Photoinduced Electron Transfer in Supramolecular Systems for Artificial Photosynthesis. *Chem. Rev.* **1992**, *92*, 435−461.

(15) Maeda, M. *Laser Dyes: Properties of Organic Compounds for Dye Lasers*; Academic Press: New York, 1984.

(16) Kim, Y.-H.; Youk, J.-S.; Kim, S. H.; Chang, S.-K. Solvatochromic Fluorescence Behavior of 8-Aminoquinoline-Benzothiazole: A Sensitive Probe for Water Composition in Binary Aqueous Solutions. *Bull. Korean Chem. Soc.* **2005**, *26*, 47−50.

(17) Weiner, A. L.; Fixler, Z. C. Topical Use of Nitrofurazone (Furacin) For Bacterial Dermatitides; effectiveness of therapy and incidence of hypersensitivity reactions. *JAMA, J. Am. Med. Assoc.* **1959**, *169*, 346−347.

(18) Pécoul, B.; Varaine, F.; Keita, M.; Soga, G.; Djibo, A.; Soula, G.; Abdou, A.; Etienne, J.; Rey, M. Long-acting chloramphenicol versus intravenous ampicillin for treatment of bacterial meningitis. *Lancet* **1991**, *338*, 862−866.

(19) Nathan, N.; Borel, T.; Djibo, A.; Evans, D.; Djibo, S.; Corty, J.; Guillerm, M.; Alberti, K.; Pinoges, L.; Guerin, P.; Legros, D. Ceftriaxone as effective as long-acting chloramphenicol in short-course treatment of meningococcal meningitis during epidemics: a randomised non-inferiority study. *Lancet* **2005**, *366*, 308−313.

(20) Jawetz, E.; Hopper, J. M. D., Jr.; Donald, R.; Smith, M. D. Nitrofurantoin in Chronic Urinary Tract Infection. *Arch. Intern. Med.* **1957**, *100*, 549−557.

(21) Dupont, H. L.; Ericsson, C. D.; Galindo, E.; Wood, L. V.; Morgan, D.; Bitsura, J. A.; Mendiola, J. G. Mendiola, Furazolidone Versus Ampicillin in the Treatment of Traveler's Diarrhea. *Antimicrob. Agents Chemother.* **1984**, *26*, 160−163.

(22) Dhaneshwar, N. N.; Kulkarni, A. G.; Tavale, S. S.; Pant, L. M. The crystal structure of a second modification of m-nitrobenzoic acid. *Acta Crystallogr., Sect. B: Struct. Crystallogr. Cryst. Chem.* **1975**, *31*, 1978−1980.

(23) Jung, Y.-J.; Jeong, Y.-S.; Seong, C.-M.; Park, N.-S. An Efficient Synthesis of 3-Substituted Quinazolones. *Bull. Korean Chem. Soc.* **1998**, *19*, 1117−1119.

(24) Shariat, M.; Abdollahi, S. Synthesis of Benzoxazinone Derivatives: A New Route to 2-(N-Phthaloylmethyl)-4H-3,1-benzoxazin-4-one. *Molecules* **2004**, *9*, 705−712.

(25) Fu, H.; Liu, Y.; Zeng, H. Shape-persistent H-bonded macrocyclic aromatic pentamers. *Chem. Commun.* **2013**, *49*, 4127−4144.

(26) France, R. R.; Cumpstey, I.; Butters, T. D.; Fairbanks, A. J.; Wormald, M. R. Fluorescence labelling of carbohydrates with 2-aminobenzamide (2AB). *Tetrahedron: Asymmetry* **2000**, *11*, 4985−4994.

(27) Paul, D. Research on heavy metal pollution of river Ganga: A review. *Ann. Agrar. Sci.* **2017**, *15*, 278−286.

(28) Cao, M.; Li, Y.; Zhao, Y.; Shen, C.; Zhang, H.; Huang, Y. A novel method for the preparation of solvent-free, microwave-assisted and nitrogen-doped carbon dots as fluorescent probes for chromium (VI) detection and bioimaging. *RSC Adv.* **2019**, *9*, 8230−8238.

(29) Dang, D. K.; Sundaram, C.; Ngo, Y.-L. T.; Chung, J. S.; Kim, E. J.; Hur, S. H. One pot solid-state synthesis of highly fluorescent N and S co-doped carbon dots and its use as fluorescent probe for Ag^{+} detection in aqueous solution. *Sens. Actuators, B* **2018**, *255*, 3284−3291.

(30) Rai, U. S.; Singh, M.; Rai, R. N. Remarkable dielectric properties of 1: 2 intermolecular compound of 2-(4-(dimethylamino) benzylideneamino) benzoic acid and urea due to excited-state intramolecular proton transfer. *RSC Adv.* **2017**, *7*, 34382−34391.

(31) Neupane, U.; Rai, R. N. Synthesis, Spectral Characterization, Thermal and OpticalStudies of Novel Complexes: 4-(Dimethylamino)-benzylidene-4-acetamideaniline and 4-(Dimethylamino)benzylidene-4-nitroaniline. *J. Fluoresc.* **2017**, *27*, 2263−2277.

(32) Kanışkan, N.; Kökten, Ş.; Çelik, İ. A new protocol for the synthesis of primary, secondary and tertiary anthranilamides utilizing N-(2 aminoarylacyl)benzotriazoles. *ARKIVOC* **2012**, *2012*, 198−213.

https://doi.org/10.1021/acsomega.1c04282
ACS Omega 2022, 7, 7460−7471

(33) Gunashekar, G. S.; Krishna, M. An Overview on Powder X-Ray Diffraction and Its Current Applications. *Res. Rev.: J. Phys.* **2015**, *4*, 6−10.
(34) Singh, M.; Rai, R. N.; Rai, U. S. Synthesis, crystal growth and physicochemical studies on a novelorganic inter-molecular compound; 3,5-dinitrobenzoic acidand salicylamide system. *J. Cryst. Growth* **2015**, *419*, 114−122.
(35) Singh, M.; Rai, R. N.; Rai, U. S. Some Physicochemical studies of organic analogue of a non metal − non metal monotectic Alloy; 2 cyanoacetamide- 4 chloronitrobenzene system. *Am. J. Anal. Chem.* **2011**, *02*, 953−961.
(36) Kalsi, P. S. *Spectroscopy of Organic Compounds*, 6th ed.; New Age Publication: India, 2005; pp 1−12.
(37) Neupane, U.; Rai, R. N. Solid state synthesis of novel charge transfer complex and studies of its crystal structure and optical properties. *J. Solid State Chem.* **2018**, *268*, 67−74.
(38) Neupane, U.; Rai, R. N. Solvent free synthesis of a novel intermolecular compound and its crystal structure, thermal and optical studies. *J. Solid State Chem.* **2018**, *265*, 1−11.
(39) Dwivedi, Y.; Kant, S.; Rai, S. B.; Rai, R. N. Synthesis, physicochemical and optical characterization of novel fluorescing complex: o-phenylenediamine—Benzoin. *J. Fluoresc.* **2011**, *21*, 1255−1263.
(40) Mataga, N.; Kaifu, Y.; Koizumi, M. Solvent Effects upon Fluorescence Spectra and the Dipolemoments of Excited Molecules. *Bull. Chem. Soc. Jpn.* **1956**, *29*, 465−470.
(41) Zachariasse, K. A.; Druzhinin, S. I.; Bosch, W.; Machinek, R. Intramolecular charge transfer with the planarized 4-aminobenzonitrile 1-tertbutyl-6-cyano-1, 2, 3, 4-tetrahydroquinoline (NTC6). *J. Am. Chem. Soc.* **2004**, *126*, 1705−1715.
(42) Do, J.; Huh, J.; Kim, E. Solvatochromic Fluorescence of Piperazine-Modified Bipyridazines for an Organic Solvent-Sensitive Film. *Langmuir* **2009**, *25*, 9405−9412.
(43) *Principles of Fluorescence Spectroscopy*; Lakowicz, J. R., Ed.; Springer Science & Business Media, 2013.
(44) Duhan, S.; Sahoo, K.; Singh, S. K.; Kumar, M. Development of Ultrasensitive and As (III) Selective Upconverting (NaYF4: Yb3+, Er3+) Platform. *Analyst* **2020**, *145*, 6378−6387.
(45) Li, P.; Hong, Y.; Feng, H.; Li, S. F. Y.; Li, Y. An efficient "off−on" carbon nanoparticle-based fluorescent sensor for recognition of chromium (VI) and ascorbic acid based on the inner filter effect. *J. Mater. Chem. B* **2017**, *5*, 2979−2988.
(46) Mondal, R. K.; Dhibar, S.; Mukherjee, P.; Chattopadhyay, A. P.; Saha, R.; Dey, B. A selective picomolar level fluorometric sensing of Cr (VI)-oxoanion in water medium by a novel metal-organic complex. *RSC Adv.* **2016**, *6*, 61966−61973.
(47) Ebrahim, S.; Shokry, A.; Khalil, M. M. A.; Ibrahim, H.; Soliman, M. Polyaniline/Ag nanoparticles/graphene oxide nanocomposite fluorescent sensor for recognition of chromium (VI) ions. *Sci. Rep.* **2020**, *10*, 13617.
(48) Dean, J. A. *Lange's Handbook of Chemistry*, 15th ed.; McGraw Hill Inc.: New York, 1999.
(49) American Public Health Association; American Water Works Association. *Standard Methods for the Examination of Water and Wastewater*; American Public Health Association, 1971.
(50) Rai, U. S.; Rai, R. N. Physical chemistry of organic eutectics. *J. Therm. Anal. Calorim.* **1998**, *53*, 883−893.

https://doi.org/10.1021/acsomega.1c04282
ACS Omega 2022, 7, 7460−7471